Estimation of Cloud Content by W-Band Radar

KENNETH SASSEN AND LIANG LIAO*

Department of Meteorology, University of Utah, Salt Lake City, Utah

(Manuscript received 2 June 1995, in final form 11 October 1995)

ABSTRACT

W-band (3.2-mm) radars are seeing increasing utilization as a result of improving microwave technologies and the increased research emphasis being given to nonprecipitating clouds. This niche is exemplified by the study of the radiatively important stratus and cirrus clouds, which essentially require the application of Rayleigh and nonspherical scattering solutions, respectively. To increase the utility of such studies, the authors provide the following relations derived from empirical and model-derived particle size distributions that rely on a combination of Rayleigh and conjugate gradient–fast Fourier transform scattering theory approaches to relate (equivalent) radar reflectivity factors (Z_e) Z ($mm^6\ m^{-3}$) to liquid water content (LWC, $g\ m^{-3}$) and ice water content (IWC, $mg\ m^{-3}$): $Z = (3.6/N_d)LWC^{1.8}$ for stratus clouds, where N_d (cm^{-3}) is the droplet concentration, and $IWC = 21.7Z_e^{0.83}$ for cirrus clouds using the dielectric constant appropriate for ice, which is valid over a IWC range of 3–100 $mg\ m^{-3}$. Sources of 95-GHz attenuation are also discussed.

In addition, radar estimates of the lidar volume extinction coefficient σ_l (m^{-1}) are derived using the exponential ice particle size distributions, yielding $\sigma_l = 6.5 \times 10^{-4}Z_e^{0.86}$ for solid ice particles, or $9.65 \times 10^{-4}Z_e^{0.81}$ if an ice density of 0.5 $g\ cm^{-3}$ is used to approximate the effects of hollow ice crystals in cirrus clouds.

1. Introduction

In view of continuing advances in short-wavelength microwave radar technologies (e.g., Pasqualucci et al. 1983; Hobbs et al. 1985; Lhermitte 1987; Mead et al. 1994), and in recognition of the need to better comprehend nonprecipitating cloud systems, radars operating at increasingly shorter wavelengths are finding application in cloud and radiation research programs. Although millimeter-wave radars have had a long history, widespread meteorological usage has not occurred until relatively recently. Primarily, this has been due to technological drawbacks and the fact that typical hydrometeor sizes in precipitation strongly call into question the use of the Rayleigh scattering approximation at these wavelengths, an unsettling proposition for traditional radar meteorologists (i.e., except those interested in hailstones). Moreover, because of the increased sensitivity to hydrometeors, microwave attenuation from precipitation can easily become a range-limiting factor. In several respects, short-wavelength radars can display both the advantages and disadvantages of lidars operating in the visible and infrared portions of the electromagnetic spectrum.

Not surprisingly, millimeter-wave radars have chiefly been applied to the research of clouds that do not generally produce rainfall: rain, and especially melting snow, can generate strong attenuation. To help determine winter mountain storm structure and a measure of cloud-top height, K-band (~1-cm) radars were incorporated into cloud seeding research projects beginning in the early 1980s (Lee 1984; Sassen 1984). Doppler radar studies in such cloud systems have proven useful for water vapor flux measurements over mountain barriers, by using relatively small ice crystals as wind tracers (Uttal et al. 1990). Similarly, Doppler K-band radar studies have yielded important insights into the internal structures of cirrus (Sassen et al. 1989) and stratus (Frisch et al. 1995) clouds. Most recently, W-band (~3-mm) Doppler radars have been applied to the study of clouds ranging from orographic cap clouds (Pazmany et al. 1994) to tornado-producing convective clouds (Bluestein et al. 1995).

The purpose of this article is to provide the best currently available means for relating W-band radar measurements to the contents of water and ice clouds. Since at the 3-mm wavelength many atmospheric targets violate the assumptions of the standard radar equation, we consider non-Rayleigh hydrometeor scattering and total atmospheric attenuation effects in order to properly treat the radar signals from clouds. Working relations between W-band radar reflectivity factors Z_e and extinction coefficients σ, and the liquid and ice mass

* Current affiliation: Caelum Research Co., Silver Spring, Maryland.

Corresponding author address: Prof. Kenneth Sassen, University of Utah, Department of Meteorology, 819 William C. Browning Building, Salt Lake City, UT 84112.

contents of clouds are offered. In addition, for the first time we examine the relation between Z_e and optical extinction coefficients in ice clouds based on exponential particle size distributions. As is the case of radar reflectivity-versus-rainfall rate relations (Battan 1973), however, we recognize that further study and validation is needed to optimize the utility of radar-derived cloud quantities from these cloud types.

2. Millimeter-wave radar probing of clouds

In consideration of many traditional radar applications, the radar equation was derived in the classic Battan (1973) textbook ignoring an attenuation term, although a chapter was devoted to the treatment of microwave attenuation, and the appropriateness of using the equivalent radar reflectivity factor Z_e under many conditions was acknowledged. For our purposes, a form of the radar equation, which, like the lidar equation, includes various sources of attenuation, is integral:

$$P_r(R) = \left(\frac{C}{R^2}\right)\eta \exp\left[-2\int (k_a + k_i + k_w)dR\right], \quad (1)$$

where $P_r(R)$ is the average power returned from range R, C the radar system constant term, η the radar reflectivity, and the exponential attenuation term contains separate extinction coefficients (dB km^{-1}) for moist air (a), ice (i) and water (w) particles, as applicable.

Radar reflectivity is defined as the sum of the single particle backscattering coefficients per unit volume, which for Rayleigh scattering at wavelength λ is expressed as

$$\eta = \left(\frac{\pi^5}{\lambda^4}\right)|K|^2 \int N(D)D^6 dD, \quad (2)$$

where $|K|^2$ is the dielectric constant appropriate for either ice or water particles, which comes from $K = (m^2 - 1)(m^2 + 2)^{-1}$, where m is the scatterer complex index of refraction, D is the spherical particle diameter, and N is the particle concentration in the diameter interval from D to dD. For Rayleigh scattering, the radar reflectivity factor is simply

$$Z = \int N(D)D^6 dD. \quad (3)$$

However, for targets whose phase may not be known, or if uncertainty exists whether Rayleigh-sized spherical scatterers are exclusively present, then Z_e is calculated directly from Eqs. (1) and (2) to derive in effect a Rayleigh-equivalent hydrometeor assemblage. Normally, the refractive index for water is used in computing Z_e (Smith 1984; Sassen 1987), but in our ice cloud simulations the value appropriate for ice at 95 GHz is employed. The values for water at 10°C and ice at −10°C are $m_w = 3.076 - i1.656$ and $m_i = 1.78 - i1.442 \times 10^{-4}$, respectively (Ray 1972). In view of the potential confusion caused by the various usage of Z, it is worthwhile to make clear our usage: Z is appropriate for Rayleigh-scattering spheres and is derived directly from Eq. (3), while Z_e includes contributions from non-Rayleigh particles and is computed, like Z_i for ice spheres, using the dielectric constant for ice.

Non-Rayleigh effects similarly need to be addressed in determining the volume extinction coefficient σ for hydrometeors with dimensions comparable to the wavelength. Atmospheric attenuation at 95 GHz is essentially due to the presence of neighboring water vapor and oxygen absorption bands. For completeness, we provide in Table 1 selected values showing the dependence of k_a on temperature and relative humidity RH, using a total pressure of 101.3 kPa and the propagation model of Liebe (1985). Clearly, under warm and moist conditions W-band radar atmospheric transmission losses can be appreciable.

3. Methodology

As in our earlier work addressing K_a-band radar cloud observations (Liao and Sassen 1994, hereafter referred to as LS), particle size distributions from both empirical sources and cloud model predictions are relied on to derive working relations between W-band radar Z_e and σ, and the ice and liquid mass contents of clouds. Since details of our computational approach have been given in LS, we will provide here brief descriptions of our methods for treating the contents of typical ice and water clouds.

a. Ice clouds

The calculation of Z_e and σ is a complicated problem for the nonspherical particles found in ice clouds that contain crystals with maximum dimensions comparable to the W-band wavelength. In our approach, the backscattering and extinction cross sections are computed for various ice crystal shape models through a numerical scheme combining the conjugate gradient and fast Fourier transform (CG-FFT) method (Sarkar et al. 1986) with the Rayleigh–Gans theory approxi-

TABLE 1. W-band radar attenuation coefficients for moist air k_a (dB km^{-1}) as a function of relative humidity (RH) and temperature (K).

	k_a				
Temperature	RH = 100%	75%	50%	25%	0%
310	4.56	2.89	1.58	0.63	0.036
300	2.18	1.44	0.83	0.37	0.040
290	1.05	0.73	0.45	0.22	0.044
280	0.53	0.38	0.26	0.14	0.048
270	0.28	0.21	0.16	0.10	0.053
260	0.16	0.14	0.11	0.08	0.058

mation for ice spheroids whenever the particle dimensions are sufficiently small relative to the incident wavelength (Gans 1912). Details of our CG-FFT method, including the results of tests to maximize computational efficiency by establishing cell size, particle shape model, and Rayleigh scattering limits, were given in Liao (1993) and LS.

The ice particle size distributions used in this study are derived from the two precipitating ice crystal datasets reported in Sato et al. (1981), obtained at the ground from South Pole station in Antarctica at temperatures similar to those in some cirrus clouds. These data were expressed as exponential size distributions of the melted ice crystal diameters as a function of precipitation intensity R_i (mm h^{-1}). Most of the sampled ice crystals were solid and hollow columns, and bullet rosettes, again consistent with cirrus clouds. Our approach converts the size distributions, over the valid range of $0.0036 \leq R_i \leq 0.16$ mm h^{-1}, to ice crystal populations of the same mass consisting in each case of column, plate, and bullet rosette models, plus a likely combined habit scenario (see LS) indicated to occur frequently in cirrus clouds. Ice crystal axial ratios varied by habit according to the dimensional relationships of Pruppacher and Klett (1978). After performing scattering simulations for each of the various habits over the measured size ranges, a regression analysis was applied to the entire dataset to obtain the relations between the computed Z_e and σ, and ice water content (IWC, mg m^{-3}), which is calculated for nonspherical particles using the equivalent volume diameter. Moreover, since we also deal with the Mie extinction behavior of the same particles for application to lidar probing, we compute the optical extinction coefficient σ_l by summing over a unit volume the extinction cross sections of each particle, which is assumed to be equal to the equivalent surface-area diameter of the nonspherical particle.

It is important to note that no ice crystal aggregates are treated in this study from either an empirical or theoretical standpoint, and that all the scattering simulations reported here are based on a vertically pointing radar system, such that the generally small elevation angle dependencies (negligible for incident horizontal polarization, see LS) attributable to our treatment of oriented particles are neglected.

b. *Water clouds*

For the spherical droplets in nonprecipitating water clouds, the calculation of Z and σ are easily solved through the use of the Rayleigh scattering approximation, since cloud droplet sizes remain much smaller than even the W-band radar wavelength. Although a great body of cloud droplet size distribution measurements from various water clouds now exists, our approach has been to apply a one-dimensional adiabatic cloud model (Sassen et al. 1992) to generate realistic cloud droplet size distributions that evolve with height as functions of temperature, updraft velocity, and cloud condensation nucleus (CCN) type and concentration. A large number of model simulations under a range of conditions appropriate for maritime and continental stratus cloud were run, and the resulting droplet size distributions were then converted to Z and liquid water content (LWC, g m^{-3}). The final relation was obtained after regression analysis employing the entire dataset as a function of the cloud droplet concentration N_d (see LS).

4. Results

a. *Z versus LWC*

Our reanalysis of the simulated LS stratus cloud microphysical compositions demonstrates that non-Rayleigh scattering and attenuation effects at W-band frequencies remain negligible. Hence, we reiterate our previous expression showing a dependency on the cloud droplet concentration N_d (cm^{-3}):

$$Z = \left(\frac{3.6}{N_d}\right)\mathrm{LWC}^{1.8}. \tag{4}$$

Figure 1 shows that the use of $N_d \approx 100$ cm^{-3} agrees well with previous empirical research reported by Atlas (1954) and Sauvagoet and Omar (1987).

b. *Z_e versus IWC*

The result of the regression analysis of the diverse habits simulated, which only produced a scatter of about 2.0 in IMC, is shown in Fig. 2. The derived relation is,

$$\mathrm{IWC} = 21.7 Z_e^{0.83}. \tag{5}$$

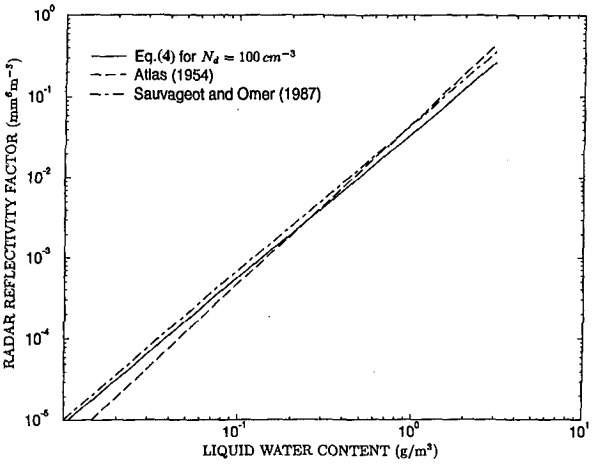

FIG. 1. Comparison of the W-band radar Z–LWC relation, using N_d = 100 cm^{-3}, with the indicated empirical relations from cumulus and stratus clouds.

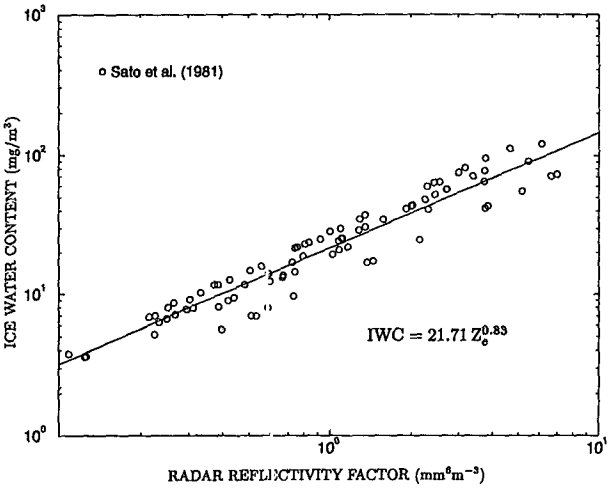

FIG. 2. The relation between W-band radar equivalent radar reflectivity factor Z_e and IWC for the ice crystal size distributions of Sato et al. (1981). The regression analysis results are shown.

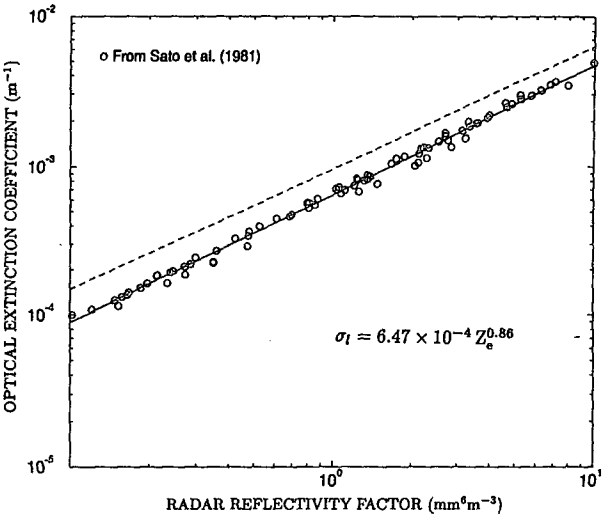

FIG. 4. Relation derived through regression analysis between W-band radar Z_e and optical (lidar) extinction coefficient σ_l, based on the Sato et al. (1981) ice crystal dataset, using an ice density of 0.92 g cm^{-3}. Dashed line shows the effect of decreasing the bulk ice crystal density to 0.5 g cm^{-3} to mimic hollow cirrus particle forms.

c. *Sources of radar extinction*

In addition to the previously delineated atmospheric propagation effects, 95-GHz extinction in water- and ice-phase clouds can also be significant. For example, we express the attenuation coefficient k_w (dB km^{-1}) of our modeled water clouds in terms of the cloud liquid water content LWC as

$$k_w = a_w(\mathrm{LWC}), \tag{6}$$

where a_w is a temperature-dependent constant that has values of 5.133, 4.796, 4.348, and 3.828 at temperatures of −10°, 0°, 10°, and 20°C, respectively.

The Sato et al. (1981) ice crystal dataset has yielded the Z_e versus σ (m^{-1}) relation shown in Fig. 3. The relation,

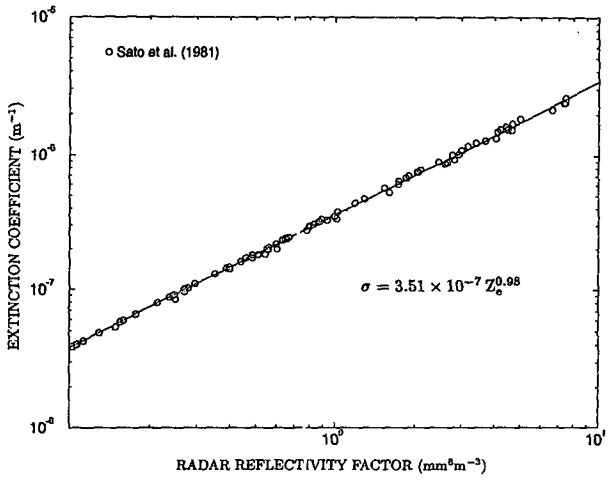

FIG. 3. W-band radar Z_e versus ice cloud extinction coefficient relation derived through regression analysis of Sato et al. (1981) data.

$$\sigma = 3.5 \times 10^{-7} Z_e^{0.98}, \tag{7}$$

indicates that non-Rayleigh effects do not generate significant departures from the expected linear σ–Z_e relationship. These relations allow for the correction of water and ice cloud attenuation on retrieved W-band radar data quantities.

d. *Z_e versus optical extinction*

Relying on the above assumptions for microwave backscattering and optical extinction, we have estimated the relation between W-band radar Z_e and visible-wavelength lidar attenuation coefficient (m^{-1}), as is shown in Fig. 4. This relation is

$$\sigma_l = 6.5 \times 10^{-4} Z_e^{0.86}, \tag{8}$$

assuming that the ice particles are solid with a density of 0.92 g cm^{-3}.

5. Discussion of uncertainties

a. *Approximate theories*

Although the use of Rayleigh scattering theory for the size range of cloud droplets simulated here, as well as Rayleigh–Gans theory for the ellipsoidal ice crystal models through the range of sizes and axial ratios found to be appropriate through our sensitivity tests is justifiable, we acknowledge that the application of the CG-FFT method in the Rayleigh–Mie theory transition zone represents an approximate approach. Nonetheless, the assuredly greater uncertainties resulting from the treatment of "equivalent" spherical ice particles have been avoided, while in reality only a small portion of

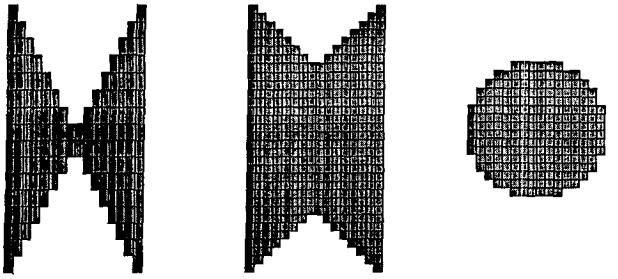

FIG. 5. Models used in the CG-FFT method simulation of hollow column ice crystal backscattering and extinction of type 1 (left) and 2: an end-on view of the column model is shown at right.

the (largest) ice crystals required non-Rayleigh CG-FFT-based corrections. As pointed out in LS, a major advantage in our treatment of ice clouds lies in the realization of the "Atlas effect," which states that randomly oriented ellipsoidal Rayleigh scattering particles will invariably produce more backscattering than a population of equivalent-volume spheres (Atlas et al. 1953).

b. Adiabatic cloud model assumptions

The model predictions of water cloud content take into account detailed microphysical and thermodynamic processes, but it should be acknowledged that other basic processes, such as dry-air entrainment and the production through coalescence of drizzle-sized drops that affect the evolution of the cloud droplet size distribution are not treated. The reasonable agreement between our cloud model predictions for droplet concentrations on the order of 100 cm^{-3} with previous Z–LWC relations from empirical studies (Fig. 1) suggests that the net effect of such processes produces a large-droplet tail in the size spectra that is fairly independent of the CCN concentration.

c. Ice crystal measurement technique

Unlike airborne 2D-probe shadow data, the ground-based ice crystal melted diameter measurements of Sato et al. (1981) directly yielded the mass distributions of precipitating ice crystals with IWCs similar to those in cirrus clouds. This avoids significant uncertainties associated with other in situ sampling methods (see discussion below). Moreover, the exponential form of these relations readily lend themselves to numerical treatment—other approaches rely on the specification of both the shape of the distribution and some mean or effective particle size.

d. Ice particle density uncertainties

Cirrus cloud particle impaction samples have shown that the vast majority of column and bullet rosette crystals display internal cavitations (Sassen et al. 1994). To investigate the effects of crystal density on radar scattering and extinction, a series of CG-FFT calculations were performed comparing solid with hollow columns of two types. The hollow column models are shown in Fig. 5 in terms of c axis cross sections, along with an end-on column view, and the results are tabulated in Table 2. Note that D_{max} refers to the major axis length of the solid column only, because the sizes of the hollow columns were increased proportionally to be of equivalent mass. When normalized in this manner, it is apparent that hollow nonspherical ice particles scatter and attenuate microwaves about the same as solid particles of the same mass, even for the relatively large cirrus cloud particles treated here. This has long been assumed with regard to the scattering properties of the air–ice mixtures of snowflakes based on the application of the Debye mixing theory (Battan 1973).

Thus, it seems appropriate to ignore the original density of the ice crystals collected at the ground, and melted in order to yield their masses as in Sato et al. (1981), which can then be converted into solid crystals of various types without much error.

On the other hand, we recognize that the relation between Z_e and optical extinction [Eq. (8)] contains a potential error resulting from the effects of ice particle density. Although Z_e is reasonably independent of ice crystal density, the same is not true of optical extinction. Computation of σ_I relies on the assumption that the ice crystal cross section is equivalent to an ice sphere of the same cross-sectional area. Adjustments for hollow particles requires a correction that depends nearly linearly on the average ice particle density. Using a value of 0.5 g cm^{-3} as a more realistic alternative in recognition of the propensity for cirrus ice crystals to display internal cavities, we offer the following relation:

TABLE 2. Extinction (σ_e) and backscattering (σ_b) cross sections for solid and hollow (type 1 and 2) column crystals (see Fig. 5) of the same mass in terms of the maximum dimension of the solid column, D_{max} (μm).

	Extinction cross section (m^2)			Backscattering cross section (m^2)		
D_{max}	Solid	Type 1	Type 2	Solid	Type 1	Type 2
400	2.79E−10	3.00E−10	2.88E−10	3.95E−10	4.18E−10	4.05E−10
800	1.88E−8	1.97E−8	1.93E−8	2.62E−8	2.57E−8	2.61E−8
1200	2.26E−7	2.21E−7	2.28E−7	2.89E−7	2.44E−7	2.74E−7

$$\sigma_l = 9.65 \times 10^{-4} Z_e^{0.81}. \quad (9)$$

We suggest the use of this relation for the estimation of cirrus ice cloud optical thickness using the vertical integral of radar-measured Z_e values.

6. Conclusions

With the increasing utilization of W-band radars for the study of cloud types of concern to climate research, including perhaps from an earth-orbiting platform (GEWEX 1994), working relations to equate radar reflectivity factors to radiatively important cloud quantities such as ice and liquid water paths are clearly valuable adjuncts. Our approach is based on the application of Rayleigh theory to cloud model–generated cloud droplet distributions, and a combined Rayleigh–Gans spheroidal and CG-FFT methods applied to an empirical ice crystal dataset. The bounds of Rayleigh scattering were established after sensitivity tests with each type of particle modeled to minimize the computational effort involved in the CG-FFT calculations. The results of our research to increase the utility of W-band radar cloud studies are summarized in Table 3.

Table 3 also includes a comparison of the current findings to those from LS for the available K_a-band radar relations. These results reveal small differences in the 3.2 mm versus 8.6 mm radar ice cloud relations that are mainly a result of the slightly increased impact of non-Rayleigh effects at 95 GHz, although it should be noted that the procedures and datasets differed somewhat in the two studies (see LS). In other words, the maximum particle sizes and their relative concentrations were insufficient to cause significant non-Rayleigh effects in the Sato et al. (1981) dataset. Note that in an earlier study (Sassen 1987) employing almost the same dataset as in LS, the relation $IWC = 37 Z_e^{0.696}$ was found (using the current nomenclature). The differences in this case are primarily due to the earlier treatment of the particles as ice spheres, thus ignoring the non-Rayleigh and "Atlas" effects. In contrast, the nonprecipitating water cloud relations in Table 3 remain unchanged because of the relatively small cloud droplet sizes present within the simulated clouds.

It should be noted that, in keeping with our intent to provide a set of the best currently available relations for W-band radar research, we have chosen not to treat the airborne 2D shadow probe data from ice clouds from Heymsfield and Platt (1984) as in LS, because these data display limitations in both the sampling of relatively small and large particles. The 2D-C (crystal) probe fails to properly identify particles smaller than 25–100 μm and larger than 500–800 μm: while the 2D-P (precipitation) probe may extend the maximum size to several millimeters, the limited probe sampling volume underestimates the quite low concentrations of the largest-sized particles in cirrus. Moreover, the errors involved in converting the 2D-image areas to particle volume and mass are potentially great, whereas the FSSP droplet probe data used to estimate the concentrations of ice crystals smaller than about 100 μm produced very significant increases in small ice crystal concentrations. Although the great numbers of small particles do not contribute much to radar scattering, they are very important in terms of lidar extinction. Hence, especially with regard to the use of σ_l–Z_e relations, we consider the ground-based melted mass size distributions to be more reliable and representative of cirrus or other ice clouds lacking particle aggregates. The ice relations based on the Sato et al. (1981) data are valid over a IWC range of 3–100 mg m^{-3}, which is typical of cirrus clouds that are not dominated by either small ice particles or large aggregates.

TABLE 3. Comparison of K_a- and W-band relations in terms of radar reflectivity factor Z (mm^6 m^{-3}), LWC (g m^{-3}), IWC (mg m^{-3}), and radar σ and lidar σ_l volume extinction coefficients (m^{-1}). The average ice particle density is ρ.

	K_a band	W band
Water clouds	$Z = (3.6/N_d)\mathrm{LWC}^{1.8}$*	$Z = (3.6/N_d)\mathrm{LWC}^{1.8}$
Ice clouds	$\mathrm{IWC} = 21.8 Z_e^{0.79}$*	$\mathrm{IWC} = 21.7 Z_e^{0.83}$
		$\sigma = 3.51 \times 10^{-7} Z_e^{0.98}$
$\rho = 0.92$ g cm^{-3}		$\sigma_l = 6.47 \times 10^{-4} Z_e^{0.86}$
$\rho = 0.50$ g cm^{-3}		$\sigma_l = 9.65 \times 10^{-4} Z_e^{0.81}$

* Liao and Sassen (1994).

These relations hold particular promise for complimenting lidar studies of stratus, altocumulus, and cirrus clouds to help fulfill current climate-related research needs. The indicated ability of radar to estimate ice cloud optical thickness is a potentially significant development that is currently being evaluated using polarization lidars, visible and infrared radiometers, and 95-GHz polarimetric Doppler radar at our Facility for Atmospheric Remote Sensing.

Acknowledgments. This research was supported by the Environmental Sciences Division of the U.S. Department of Energy under Grants DEFG-0394ER61747 and DE-FG02-95ER62023 as part of the Atmospheric Radiation Measurement Program, and by NSF Grant ATM-8914348.

REFERENCES

Atlas, D., 1954: The estimation of cloud content by radar. *J. Meteor.*, **11**, 309–317.

——, M. Kerker, and W. Hitschfield, 1953: Scattering and attenuation by nonspherical atmospheric particles. *J. Atmos. Terr. Phys.*, **3**, 108–119.

Battan, L. J., 1973: *Radar Observation of the Atmosphere.* University of Chicago Press, 324 pp.

Bluestein, H. B., A. Pazmany, J. C. Galloway, and R. E. McIntosh, 1995: Studies of the substructure of severe convective storms using a mobile 3-mm wavelength Doppler radar. *Bull. Amer. Meteor. Soc.*, **76**, 2155–2169.

Frisch, A. S., C. W. Fairall, and J. B. Snider, 1995: Measurement of stratus cloud and drizzle parameters in ASTEX with K_a-band

Doppler radar and microwave radiometer. *J. Atmos. Sci.,* **52,** 2788–2799.

Gans, R., 1912: Über die Form ultrmikroskopischer Goldteilchen. *Ann. Phys.,* **37,** 881–900.

GEWEX, 1994: *Utility and Feasibility of a Cloud Profiling Radar: Report of the GEWEX Topical Workshop.* ICPO Pub. Series, No. 10, WMO, 46 pp.

Heymsfield, A. J., and C. M. R. Platt, 1984: A parameterization of the particle size spectrum of ice clouds in terms of ambient temperature and the ice water content. *J. Atmos. Sci.,* **41,** 846–855.

Hobbs, P. V., N. T. Funk, R. R. Weiss, J. D. Locatelli, and K. R. Biwas, 1985: Evaluation of a 33 GHz radar for cloud physics research. *J. Atmos. Oceanic Technol.,* **2,** 35–48.

Lee, R. R., 1984: Two case studies of wintertime cloud systems over the Colorado Rockies. *J. Atmos. Sci.,* **41,** 868–878.

Lhermitte, R., 1987: A 94-GHz Doppler radar for cloud observations. *J. Atmos. Oceanic. Technol.,* **4,** 36–48.

Liao, L., 1993: K_a-band radar research applications for ice and water clouds. Ph.D. dissertation, University of Utah, 220 pp.

——, and K. Sassen, 1994: Investigation of relationships between K_a-band radar reflectivity and ice and water contents. *Atmos. Res.,* **34,** 231–248.

Liebe, H. J., 1985: An updated model for millimeter wave propagation in moist air. *Radio Sci.,* **20,** 1069–1089.

Mead, J. B., A. L. Pazmany, S. M. Sekelsky, and R. E. McIntosh, 1994: Millimeter-wave radar for remotely sensing clouds and precipitation. *Proc. IEEE,* **82,** 1891–1906.

Pasqualucci, F., B. Bartram, R. A. Kropfli, and W. R. Moninger, 1983: A millimeter-wavelength dual-polarization Doppler radar for cloud and precipitation studies. *J. Climate Appl. Meteor.,* **22,** 758–765.

Pazmany, A. L., J. B. Mead, R. E. McIntosh, M. Hervig, R. Kelly, and G. Vali, 1994: 95 GHz polarimetric radar measurements of orographic cap clouds. *J. Atmos. Oceanic Technol.,* **11,** 140–153.

Pruppacher, H. R., and J. D. Klett, 1978: *Microphysics of Clouds and Precipitation.* D. Reidel, 714 pp.

Ray, P. S., 1972: Broadband complex refractive indices of ice and water. *Appl. Opt.,* **11,** 1836–1844.

Sarkar, T. K., E. Arvas, and S. M. Rao, 1986: Application of FFT and the conjugate gradient method for the solution of electromagnetic radiation from electrically large and small conducting bodies. *IEEE Trans. Antennas Propag.,* **34,** 634–640.

Sassen, K., 1984: Deep orographic cloud structure and composition derived from comprehensive remote sensing measurements. *J. Climate Appl. Meteor.,* **23,** 568–583.

——, 1987: Ice cloud content from radar reflectivity. *J. Climate Appl. Meteor.,* **26,** 1050–1053.

——, D. O'C. Starr, and T. Uttal, 1989: Mesoscale and microscale structure of cirrus clouds: Three case studies. *J. Atmos. Sci.,* **46,** 371–396.

——, H. Zhao, and D. C. Dodd, 1992: Simulated polarization diversity lidar returns from water and precipitating mixed phase clouds. *Appl. Opt.,* **31,** 2914–2923.

——, N. C. Knight, Y. Takano, and A. J. Heymsfield, 1994: Effects of ice-crystal structure on halo formation: Cirrus cloud experimental and ray-tracing modeling studies. *Appl. Opt.,* **33,** 4590–4601.

Sato, N., K. Kikuchi, S. C. Barnard, and A. W. Hogan, 1981: Some characteristic properties of ice crystal precipitation in summer season at South Pole Station, Antarctica. *J. Meteor. Soc. Japan,* **59,** 772–780.

Sauvageot, H., and J. Omar, 1987: Radar reflectivity of cumulus clouds. *J. Atmos. Oceanic Technol.,* **4,** 264–272.

Smith, P. L., 1984: Equivalent radar reflectivity factors for snow and ice particles. *J. Climate Appl. Meteor.,* **23,** 1258–1260.

Uttal, T., J. B. Snider, R. A. Kropfli, and B. W. Orr, 1990: A remote sensing method of measuring atmospheric vapor fluxes: Application to winter mountain storms. *J. Appl. Meteor.,* **29,** 22–34.